

Isaac G. Wright, Josemaria Gomez Sócola, and Fabiano S. Rodrigues
The University of Texas at Dallas, W. B. Hanson Center for Space Sciences, Richardson, TX

1. INTRODUCTION & MOTIVATION

- Low-latitude scintillation can be described as the manifestation of fast-moving and time-evolving diffraction patterns created by ionospheric irregularities associated with Equatorial Spread F.
- It has been proposed that the orientation of these scintillation patterns can be determined from the direction of the signal and the orientation of the magnetic field.
- Theoretical and experimental studies of the orientation of scintillation fade patterns are key for spaced-receiver scintillation measurements and the interpretation of these measurements with respect to the irregularities causing the fades.

2. PROJECT GOALS

- Given that previous attempts to analyze the orientation of scintillation patterns have some inconsistencies, we designed a project with the following goals:
 - (G1) Revisit theoretical models of scintillation pattern orientation and generalize them to more realistic receiver configurations.
 - (G2) Conduct an experiment to compare the results of our theoretical approach with real (i.e., measured) scintillation patterns.

3. BACKGROUND INFORMATION

- Kintner et al. (2004) deployed an array of GNSS receivers in Brazil to characterize scintillation fade patterns. They developed a model that was able to account for ~1/3 of orientations observed by the receivers.
- Despite further investigation, no explanation was found to explain discrepancies in data when the position vector was within 60° of the magnetic vector.
- Orientation was later expanded upon by Ledvina et al. (2004) in an effort to determine plasma drifts using the spaced receiver method.
 - No experimental validation of their updated approach for orientation was performed.
 - A realistic receiver setup needs to be considered.
 - Should the 60° cone still be considered?

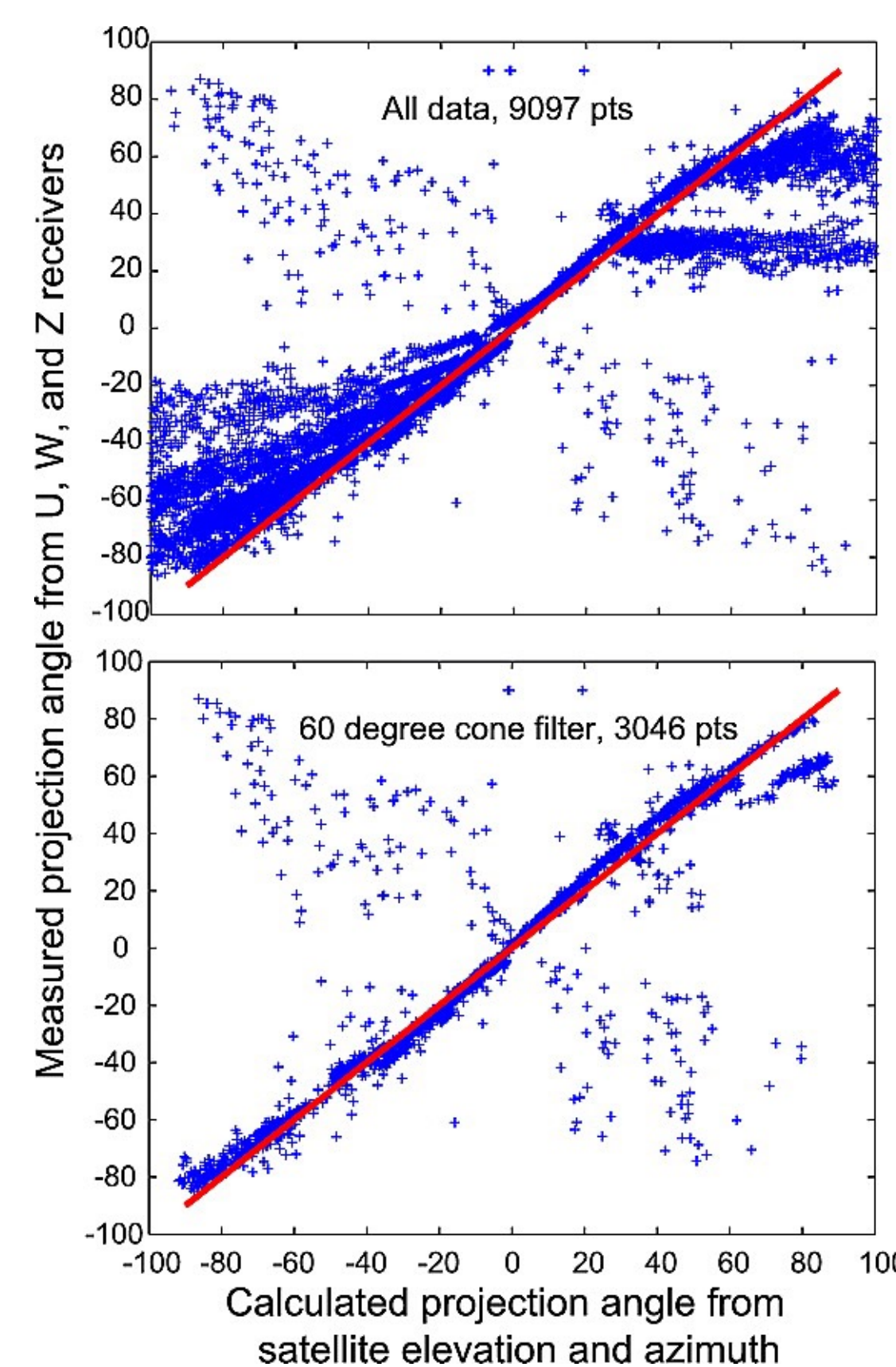


Figure 1: Modeled vs measured orientations for all points (top) and only for points separated by at least 60° from the magnetic field (bottom) (From Kintner et al., 2004).

4. PROJECTION BASED MODEL OF ORIENTATION

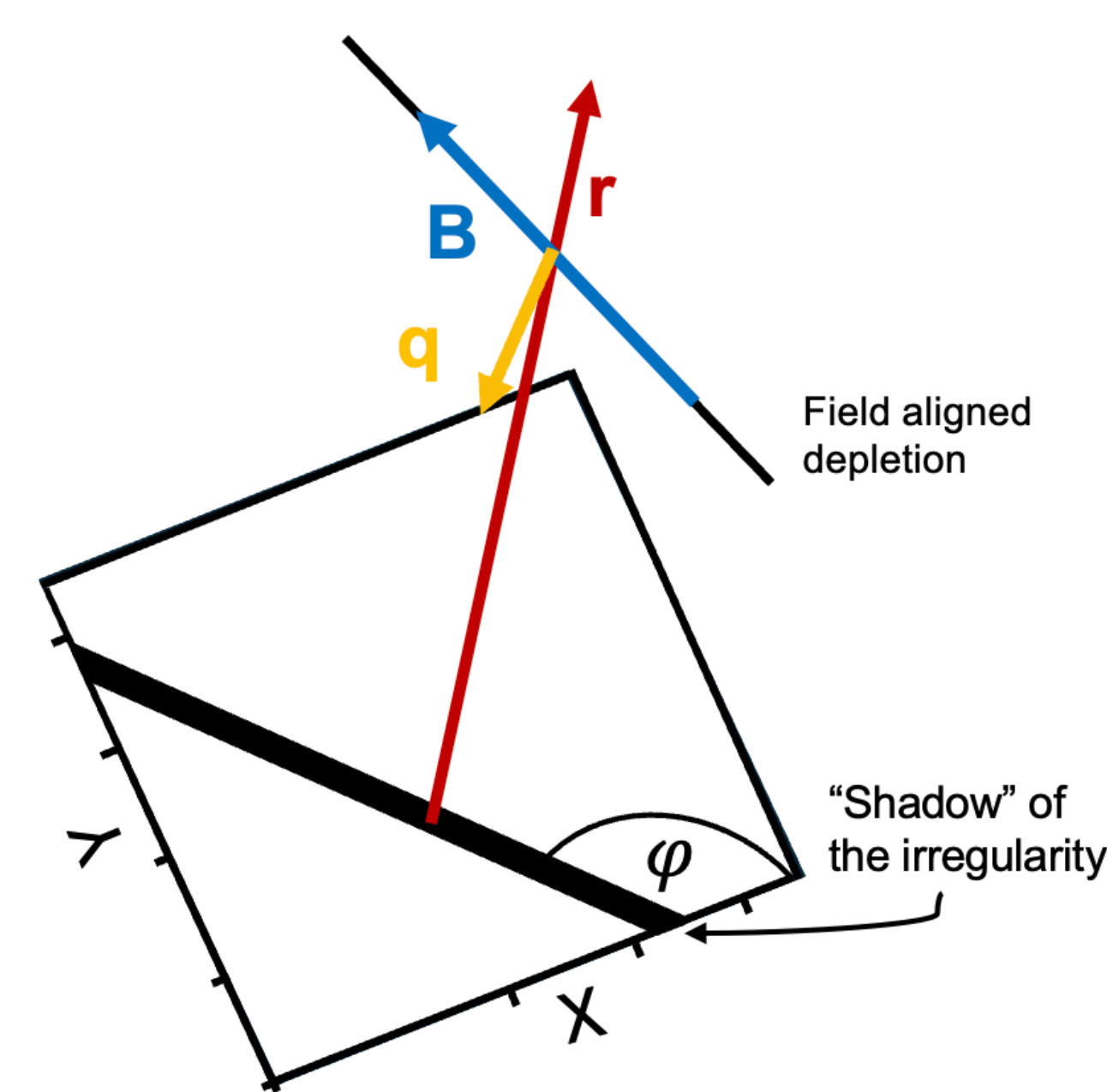


Figure 2: Depiction of projection geometry.

- Diffraction occurs from the perspective of the propagating signal incident upon the irregularity.
- Per the equipotential assumption, plasma irregularities are assumed to “map” along \vec{B} (Farley, 1960).
- Therefore, diffraction should be centered about both \vec{r} and \vec{B} , represented by a plane with normal vector \vec{q} (Ledvina et al., 2004):

$$\vec{q} = \vec{r} \times \vec{B} \quad (1)$$
- We obtain \vec{B} using IGRF-13 and by assuming a thin spherical shell ionosphere model at a height of 350km.
- The orientation of this plane’s intersection with the ground plane is the projection angle φ and can be determined as:

$$\varphi = \arctan\left(\frac{-q_x}{q_y}\right) + \pi \quad (2)$$

5. EXPERIMENTAL SETUP

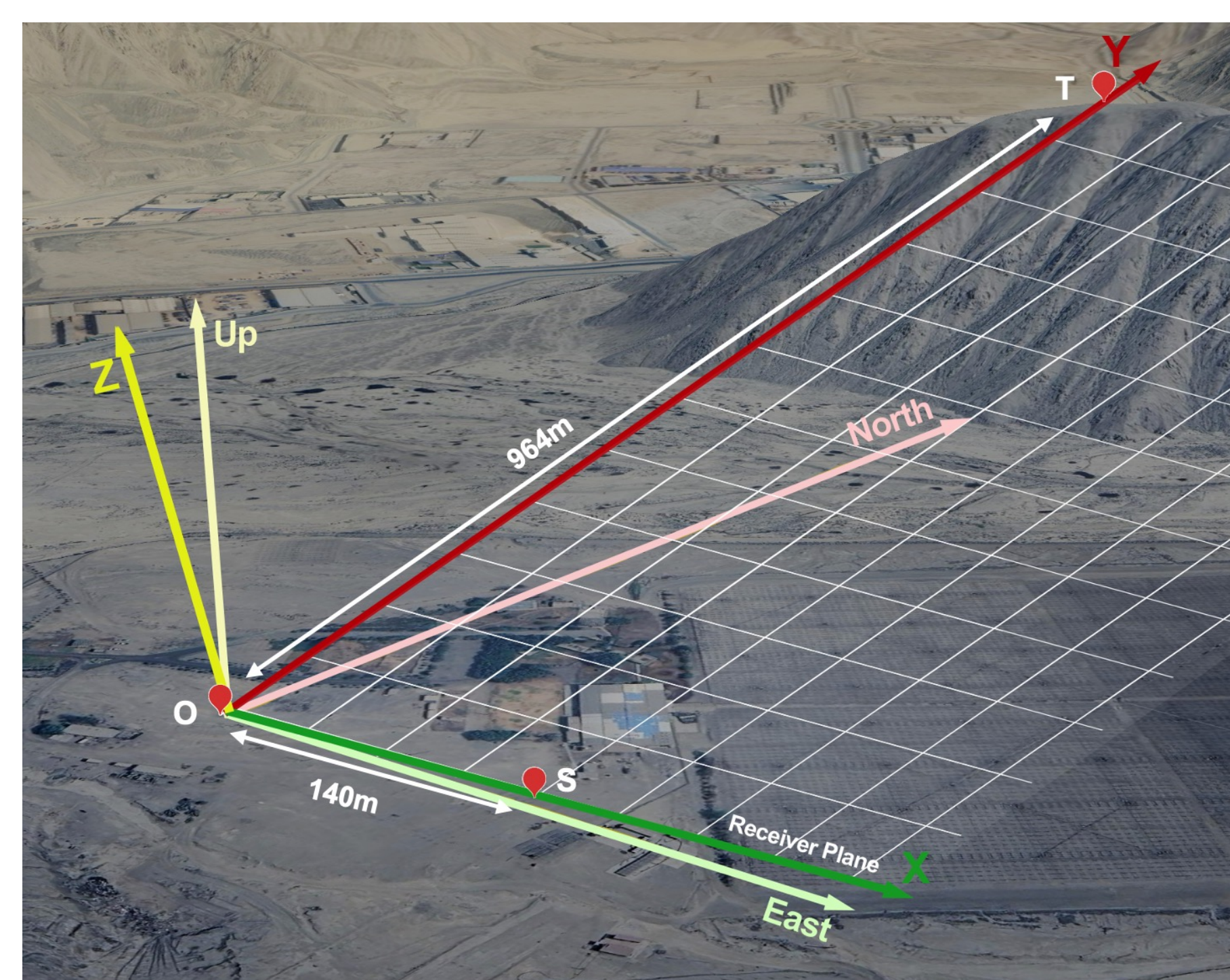


Figure 3: Receiver array at the Jicamarca Radio Observatory. We show axes of the geographic East North Up (ENU) coordinate system in light colors and axes of the receiver coordinate system in dark.

- We operated three GNSS-based scintillation monitors – ScintPi (Gomez Sócola and Rodrigues, 2022) during March 10-19, 2023, at the Jicamarca Radio Observatory.
 - Located in Peru (11.97° S, 76.87° W, ~1.3° inclination)
 - 20 Hz multi-constellation, carrier to noise (C/No) measurements were collected from receivers labeled T, O, and S in Figure 3.
- Receivers vary in altitude. Therefore, we must consider projection not onto the ground plane but instead a tilted surface which we refer to as the receiver plane.
- To correct for this bias, we construct the “receiver coordinate frame”:
 - Cartesian coordinate system oriented such that receivers T, O, and S lie in the xy-plane, and the y-axis is along T and O.
 - Two baselines approximately 964m in y and 140m in x.

6. METHODOLOGY

- Orientation in the receiver frame can be determined by assuming the fade surface as a plane wave with velocity \vec{V} and projection angle φ related to wavevector \vec{k} (Kintner et al., 2004):

$$\vec{k} = \langle \sin(\varphi), -\cos(\varphi) \rangle$$

$$\vec{V} \cdot \vec{k} = \frac{\vec{OT} \cdot \vec{k}}{\tau_{OT}} = \frac{\vec{OS} \cdot \vec{k}}{\tau_{OS}}$$

$$\Rightarrow \tan(\varphi) = \frac{\tau_{OT}\vec{OS}_y - \tau_{OS}\vec{OT}_x}{\tau_{OT}\vec{OS}_y - \tau_{OS}\vec{OT}_x} \quad (3)$$

Where τ_{OT} and τ_{OS} represent the time lags between \vec{OT} and \vec{OS} . Note that \vec{OT}_x is 0 in the receiver frame.

- To obtain time lag τ , we performed cross correlation analyses of C/No (60s bins with a cadence of 5s).
- To minimize the impact of multipath in the analysis, data points were only considered where $S_4 > 0.2$, $\rho > 0.7$, and elevation $> 10^\circ$.
- The angle obtained with the above method is in the receiver plane. Therefore, to compare the modeled angle (1) with these results, we transform \vec{q} to the receiver frame, making use of $ENU \rightarrow ECEF$, and $ENU \rightarrow RX$ rotation matrices.

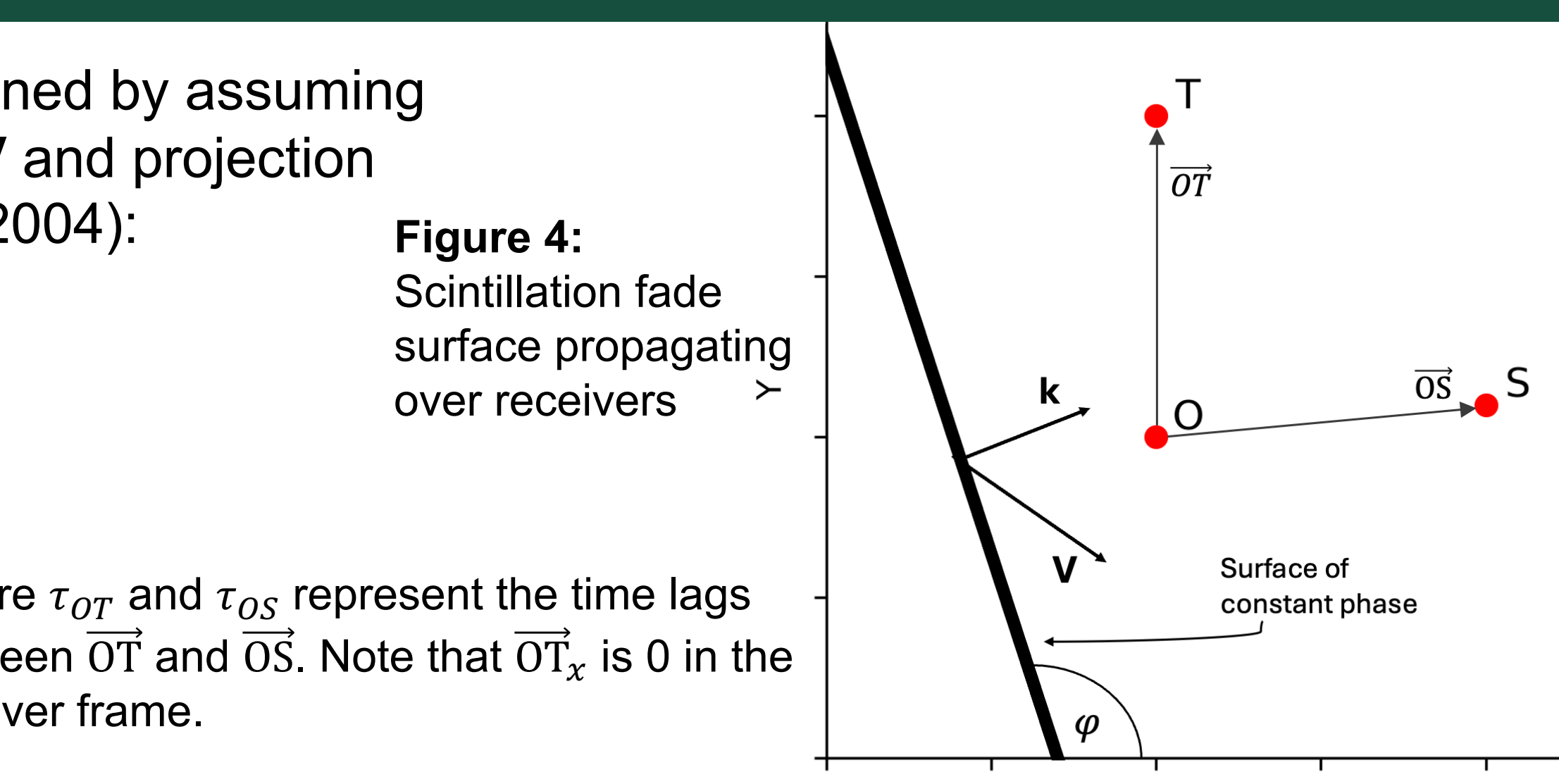


Figure 4: Scintillation fade surface propagating over receivers

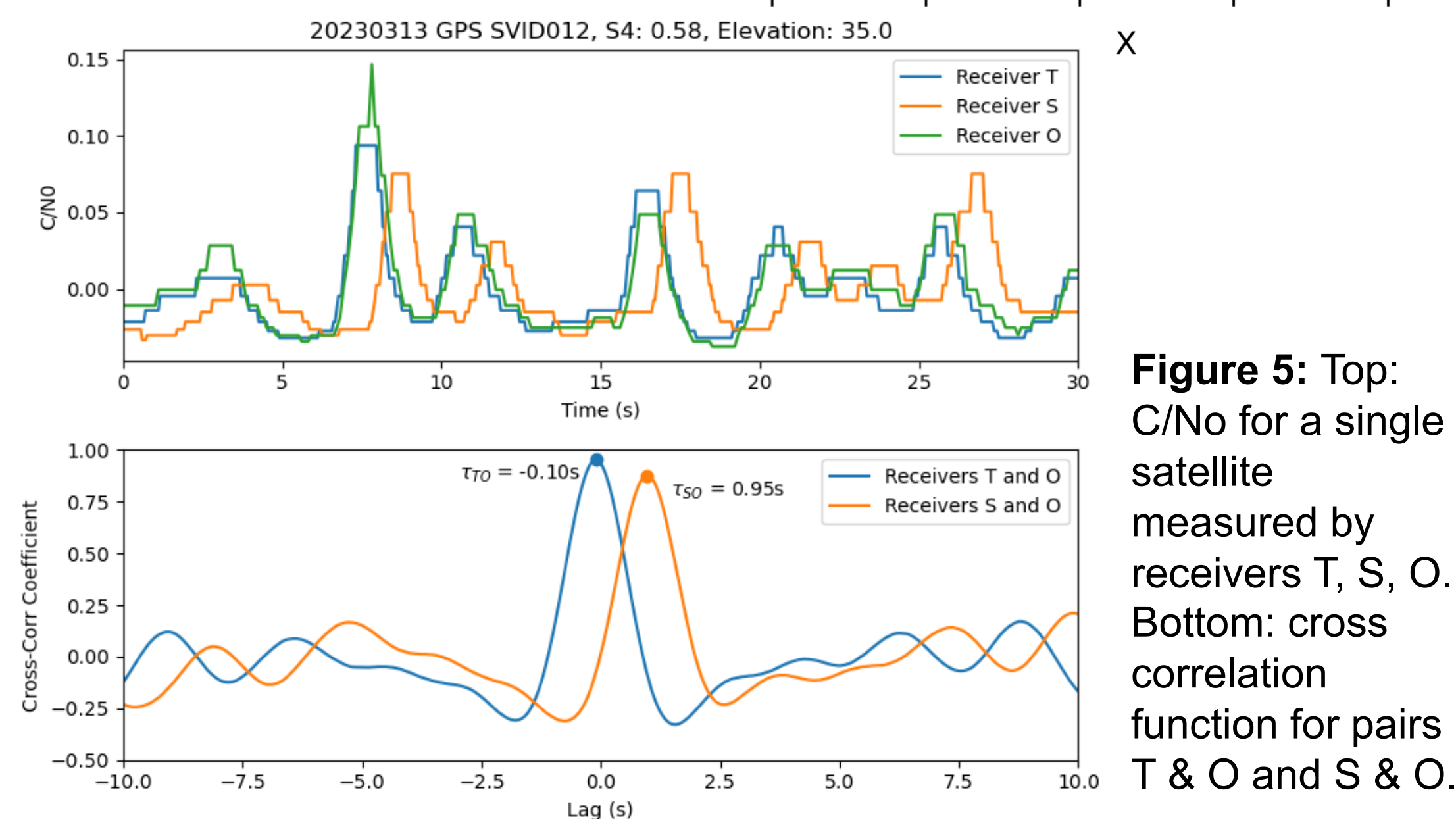


Figure 5: Top: C/No for a single satellite measured by receivers T, S, O. Bottom: cross correlation function for pairs T & O and S & O.

7. RESULTS

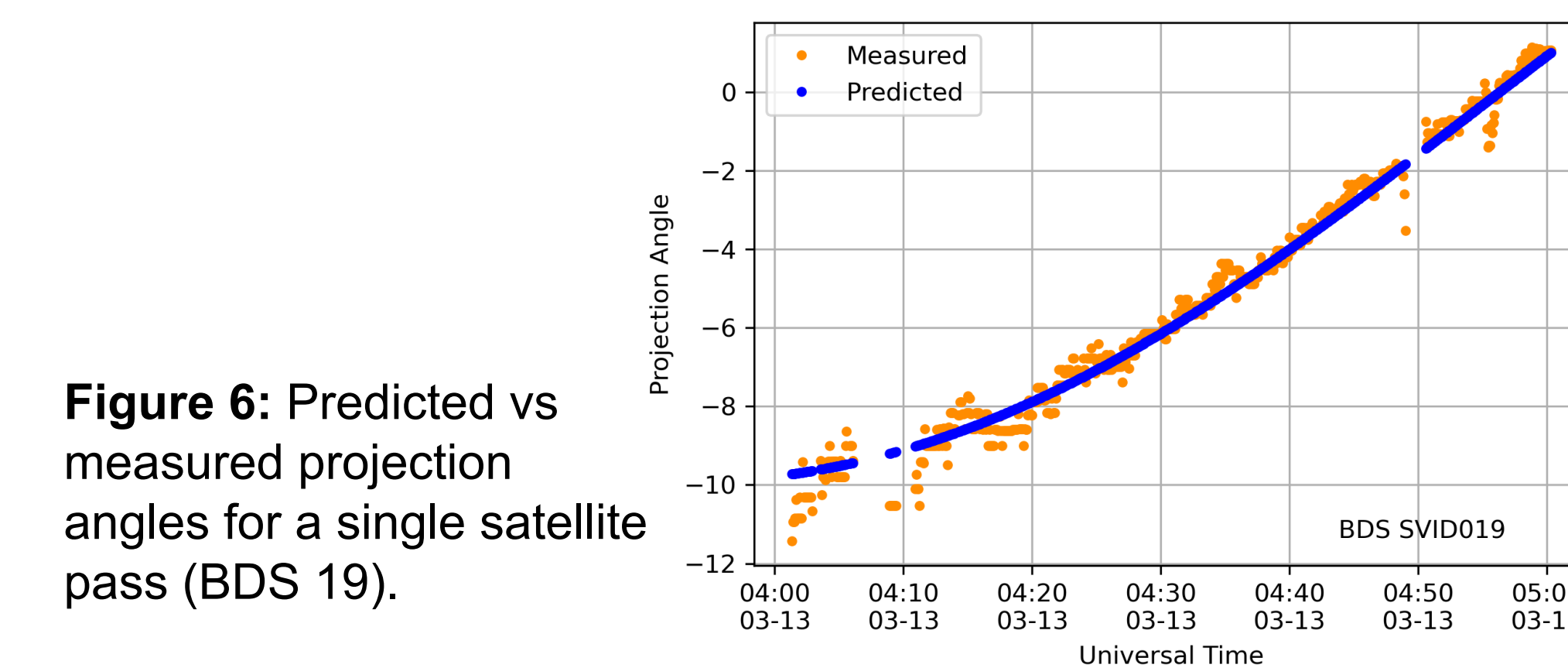


Figure 6: Predicted vs measured projection angles for a single satellite pass (BDS 19).

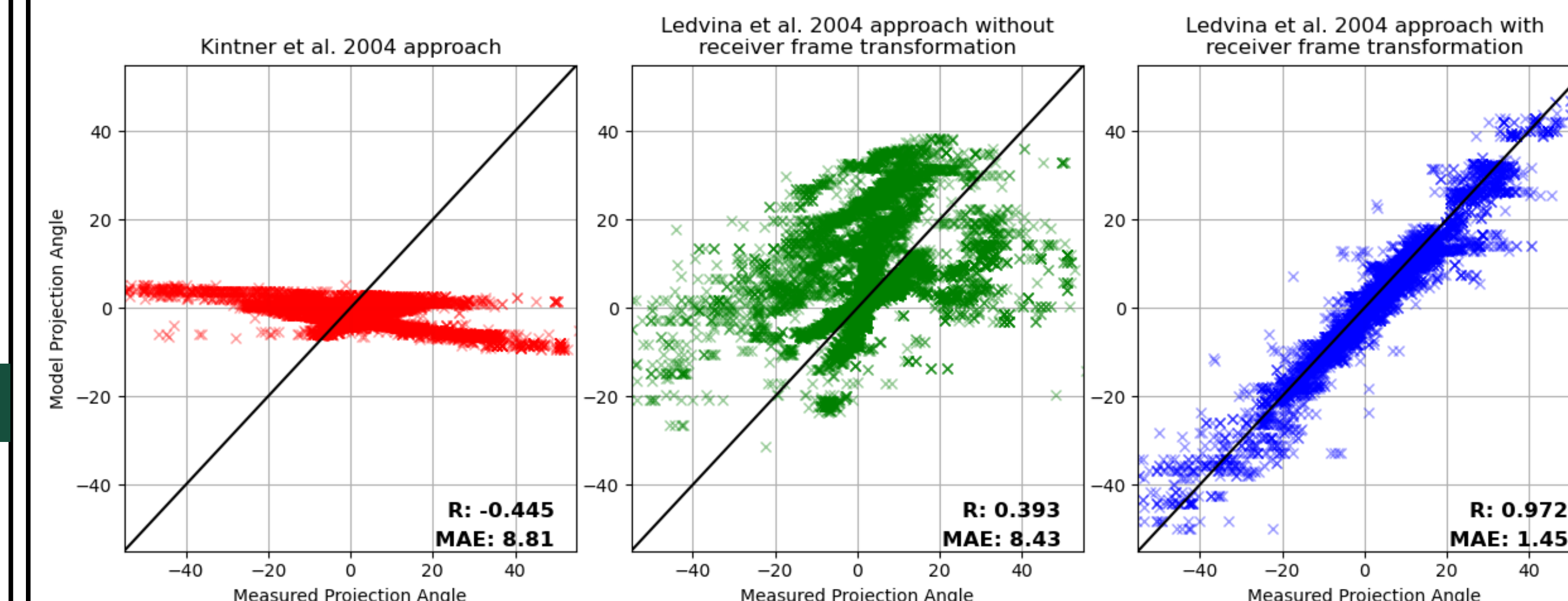


Figure 7: Comparison of the projection angle models using all campaign measurements. Pearson R and Mean Average Error (MAE) shown in corner. Black line indicates a perfect fit.

8. DISCUSSIONS

- We hypothesize that the discrepancy in Kintner et al. (2004) was due to the assumption of \vec{B} being taken at the receiver array.
 - \vec{B} should be obtained at the ionospheric pierce point.
 - This error is most prominent when \vec{r} and \vec{B} are closer to parallel.
 - This is supported by our experiment for which virtually all the data were in the 60° cone. The magnetic dip at the array site was ~0°, yielding angles of nearly 0° as per the original formulation.
- Most of the remaining disagreements can be attributed to multipath, limited measurement resolutions, and uncertainty in assuming scattering height.

9. CONCLUSIONS

- We generalized the scintillation projection model proposed by Ledvina et al. (2004) to account for projection onto a tilted surface. (G1)
- Using an array of GNSS-based receivers, we were able to measure orientation angles of scintillation patterns. The results are consistent with our projection-based model. (G2)
- The work presented here contributes to a better understanding and modeling of observed scintillation fade patterns with implications for studies relating observed scintillation patterns and the irregularities responsible for them.
- Finally, the work exemplifies the benefits of low-cost scintillation monitor options for spaced-receiver studies.

REFERENCES

- Farley DT. 1960. Electrostatic fields in the ionosphere at non-polar geomagnetic latitudes. *J. Geophys. Res.* 65(3): 869–877.
- Gomez Socola J, Rodrigues FS. 2022. ScintPi 2.0 and 3.0: GNSS-based monitors of ionospheric scintillation. *Earth Planets Space*, 74, 185.
- Kintner, P. M., B. M. Ledvina, E. R. de Paula, and I. J. Kantor (2004). Size, shape, orientation, speed, and duration of GPS equatorial anomaly scintillations, *Radio Sci.*, 39, RS2012.
- Ledvina, B. M., P. M. Kintner, and E. R. de Paula (2004). Understanding spaced-receiver zonal velocity estimation, *J. Geophys. Res.*, 109, A10306

ACKNOWLEDGEMENTS

We would like to thank the staff of the Jicamarca Radio Observatory for technical support. This material is based upon work supported by the NSF Graduate Research Fellowship Program under Grant No. (2136516), by NSF Award AGS-2122639, and by the Eugene McDermott Foundation.